


Spin accumulation dynamics in spin valves in the terahertz regime

A. Vedyayev,^{1,2,*} N. Ryzhanova,^{1,2} N. Strelkov^{1,2} ,^{1,2} A. Lobachev,² and B. Dieny^{1,†}

¹Université Grenoble Alpes, CEA, CNRS, Grenoble INP, IRIG-SPINTEC, 38000 Grenoble, France

²Department of Physics, Moscow Lomonosov State University, Moscow 119991, Russia

 (Received 27 September 2019; revised manuscript received 18 November 2019; published 2 January 2020)

The notion of spin accumulation and spin relaxation in the diffusive regime was introduced by Valet and Fert in 1993 to describe the current-perpendicular-to-plane (CPP) diffusive transport in metallic magnetic multilayers. This theory has been quite successful in explaining the giant magnetoresistance of magnetic multilayers in CPP geometry in the frequency range from DC to a few gigahertz. In this paper, we investigate the dynamic aspect of spin accumulation from the theoretical point of view when reaching the terahertz (THz) frequency range. The characteristic relaxation time of electron elastic scattering is typically in the femtosecond range. However, since spin accumulation results from a diffusion process involving a very large number of individual scattering events, the characteristic time of spin accumulation variation when the current and/or the magnetic configuration are varied can be significantly longer than that of the input signal, eventually reaching the picosecond range. In spintronic devices operating in the THz range such as those based on ferrimagnetic or antiferromagnetic materials, the spin accumulation amplitude and, correlatively, the device magnetoresistance can therefore depend on the actual device operating frequency. We investigate this question by extending the Valet and Fert theory in the time domain.

DOI: [10.1103/PhysRevB.101.014401](https://doi.org/10.1103/PhysRevB.101.014401)

I. INTRODUCTION

Since the seminal observation of ultrafast demagnetization in nickel by Beaurepaire and coworkers [1] and, more recently, the possibility of all-optical magnetization switching by femtosecond lasers [2], interest in ultrafast magnetism and the related field of terahertz (THz) spintronics has kept increasing [3–5]. Today, THz technology is used in many applications encompassing homeland security, global environmental monitoring, quality control of agriculture products and foods, biology and medical sciences, and information and communication technology [6]. It is also claimed that THz spintronics may open new avenues in computer technology by dramatically increasing the computational speeds thanks to the combination of ultrafast optics, photonics, and spintronics [3]. Ultrafast control of magnetization (picosecond scale) can be achieved by various means, including femtosecond to picosecond laser pulses, heat, and magnetic or electrical field pulses. Picosecond pulses of current can be generated by exciting bunches of hot electrons using laser pulses. Continuous (DC) current can also be used to drive steady excitations via spin transfer [7–9] or spin-orbit torques [10–12]. Various rf devices were conceived by combining the oscillatory precession of magnetic moments with giant or tunnel magnetoresistance phenomena. In particular, they enabled two basic rf functions: DC to rf conversion for rf signal generation with spin transfer oscillators [13–16] and rf to DC conversion for rf signal detection with spin diodes [17–19]. These devices commonly operate in the gigahertz

(GHz) range mostly addressing the market of the Internet of Things (IoT) with bands in the 0.3–5.5-GHz range and public mobile networks (2G–4G) using bands within 0.7–3 GHz. However, there is an increasing demand to move towards higher frequency to fulfill the requirements for 5G technology and beyond (hundreds of GHz towards THz) for the future IoT [20]. These frequencies can be reached by using ferromagnetic materials with very low damping and high anisotropy such as Heusler alloys [21] and antiferromagnetic or ferrimagnetic materials [22] wherein the excitation frequency is determined by the exchange interaction between the sublattices.

With the aim of developing spintronics devices operating at a THz frequency, it is important to get a thorough understanding of spin transport at these frequencies. Transport can be ballistic or diffusive depending on length scales and spin scattering rates and superdiffusive between these two regimes [23–25]. In the present study, we focus on the strong scattering regime for which the transport is diffusive. In magnetic metals, the transport is described by the two-current model proposed by Mott in 1936 [26]. This model assumes that as long as spin flip can be considered to be negligible (i.e., with weak spin-orbit scattering and at a temperature much below the Curie temperature), the two species of electrons with spin parallel (\uparrow) and antiparallel (\downarrow) to the local magnetization carry the current in parallel. The DC conductivity is then the sum of the conductivity of the two spin channels, the conductivity of each channel following the Drude model [27]:

$$\sigma_{\text{DC}} = \sigma_{\uparrow} + \sigma_{\downarrow} = \frac{e^2}{m} (N_{\uparrow} \tau_{\uparrow} + N_{\downarrow} \tau_{\downarrow}), \quad (1)$$

where e and m are, respectively, the conduction (sp) electron charge and effective mass, N_{\uparrow} and N_{\downarrow} are the spin-dependent

*vedy@magn.ru

†bernard.dieny@cea.fr

densities of conduction electrons at Fermi energy, and τ_{\uparrow} and τ_{\downarrow} are the spin-dependent elastic scattering times. This model was successfully used to interpret resistivity measurements in magnetic transition-metal alloys [28–31]. The elastic scattering time in transition metals is typically in the range of 10 to 100 fs, corresponding to scattering rates $\Gamma/2\pi$ of 10 to 100 THz [32]. Most of the experiments conducted in the spintronics area so far have been carried out in the DC regime or up to a frequency of a few tens of GHz, which is much below this elastic relaxation timescale. This was particularly the case in all studies related to giant magnetoresistance or tunnel magnetoresistance which yielded ultrasensitive magnetoresistive read heads used in hard-disk drives since 1997 [33]. Consequently, treating the electron transport in these experiments as being in the quasistatic regime was a good approximation. However, if the operating frequency of spintronic devices is increased up to the THz range, the characteristic time of the measurement becomes sub-picosecond and therefore much closer to the elastic scattering time. The conductivity of the system then decreases [32] and becomes complex. For each spin category, the complex frequency-dependent conductivity is then written as [34–37]

$$\sigma^{\uparrow(\downarrow)}(\omega) = \frac{\sigma_{\text{DC}}^{\uparrow(\downarrow)}}{1 - i\omega\tau^{\uparrow(\downarrow)}}, \quad (2)$$

where ω is the excitation frequency.

Terahertz spectroscopy has been shown to be a very efficient tool to separately determine the spin-dependent density of conduction electrons and spin-dependent relaxation rates [38,39] and thereby access the fundamental parameters of magnetotransport in metals.

Previously, AC magnetoresistance was theoretically investigated in Ref. [40]. The authors calculated frequency-dependent complex magnetoimpedance of a spin valve by applying harmonically oscillating voltage. Both current and spin accumulation are harmonic functions with a given frequency. But we are interested in the time evolution of spin accumulation while injecting the spin current in a spin valve with some characteristic time, and we will show that evolution of spin accumulation may be characterized by another time depending on values of the spin relaxation and spin-diffusion time.

Modern spintronics devices are often based on the current-perpendicular-to-plane (CPP) geometry [39,41–45] or on lateral geometry [46–55] in which spin accumulation and spin relaxation phenomena play a very important role [45]. The concept of spin accumulation when a current flows perpendicular to a ferromagnetic-metal/nonmagnetic-metal interface was introduced by Van Son *et al.* [56]. It was then extended to explain the CPP giant magnetoresistance (GMR) of magnetic multilayers by Valet and Fert [45]. This theory has been extensively used to interpret CPP GMR measurements in magnetic metallic multilayers taking into account bulk and interfacial spin-flip mechanisms. In steady-state CPP transport, the local spin-dependent chemical potential $\mu^{\uparrow(\downarrow)}$ obeys a diffusion equation given by [56]

$$\frac{\mu^{\uparrow} - \mu^{\downarrow}}{\tau_{\text{sf}}} = \mathcal{D} \frac{\partial^2(\mu^{\uparrow} - \mu^{\downarrow})}{\partial x^2}, \quad (3)$$

where the x axis is perpendicular to the interface, \mathcal{D} is the diffusion constant, and τ_{sf} is the spin-flip relaxation time.

From Eq. (3), the spin accumulation exponentially relaxes as a function of the distance from a magnetic/nonmagnetic interface over a characteristic spin diffusion length given by $\ell_{\text{sf}}^2 = \mathcal{D}\tau_{\text{sf}}$ [45,56].

As mentioned previously, because most of the experiments in spintronics have so far been performed at frequencies much lower than the typical diffusion rates, it has been considered that the vector of spin accumulation instantaneously follows any change in the magnetic configuration of the considered system. However, because the evolution of spin accumulation is a diffusion process, it involves a large number of individual scattering events. As a result, the timescale of the spin accumulation dynamics can be significantly longer than the timescale of elastic scattering. This is particularly true in lateral spin valves, whose dimensions can reach several hundreds of nanometers [46–55]. This corresponds to much longer diffusion distances than those usually encountered in CPP experiments in (F/NM) multilayers (F=ferromagnetic layer, NM=nonmagnetic spacer) where the diffusion distances are the thickness of the nonmagnetic spacers, typically a few nanometers. Nevertheless, in both cases (lateral spin valves or CPP multilayers), one may expect an influence of the excitation frequency on the spin accumulation dynamics when approaching the THz range, this influence making it all the more important that the length of the device (i.e., the length over which the electrons have to diffuse) is long.

It is the purpose of this paper to investigate theoretically the dynamics of spin accumulation in such systems when going beyond the steady-state approximation, i.e., entering the THz regime.

II. MODEL

To investigate the dynamic properties of multilayered spin valves, we extend the one-dimensional Valet and Fert approach by explicitly introducing a time dependence in the diffusion equation. The current is assumed to propagate along the x axis. We rewrite the currents for spin-“up” and spin-“down” electrons (see Eq. (13) in Ref. [45]) in the following form:

$$j^{\uparrow(\downarrow)} = -\sigma^{\uparrow(\downarrow)} \left(\frac{\partial u}{\partial x} + \frac{1}{eN_0} \frac{\partial n^{\uparrow(\downarrow)}}{\partial x} \right), \quad (4)$$

where $\sigma^{\uparrow(\downarrow)} = \sigma_0(1 \pm \beta)$ is the spin-dependent conductance, β is an asymmetry factor, u is the electrostatic potential, e is the absolute electron charge, N_0 is a density of states at the Fermi level per volume, and $n^{\uparrow(\downarrow)} = n_0 \pm \Delta n$ is the density of electrons with spin up and down, with n_0 being the density of electrons of each spin category at equilibrium. The first part of (4) represents the convection current due to the electric field, while the second part is the current due to diffusion. The charge current is then given by $j_e = j^{\uparrow} + j^{\downarrow}$, and the spin current is given by $j_m = j^{\uparrow} - j^{\downarrow}$. They obey the following continuity equations [57]:

$$\begin{aligned} 2e \frac{\partial n_0}{\partial t} + \nabla j_e &= 0, \\ 2e \frac{\partial \Delta n}{\partial t} + \nabla j_m &= -2e \frac{\Delta n}{\tau_{\text{sf}}} - 2e \frac{J_{\text{sd}}}{\hbar} \Delta n \sin \gamma, \end{aligned} \quad (5)$$

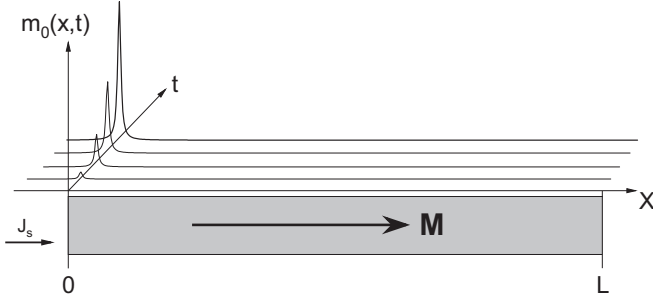


FIG. 1. Toy model consisting of a ferromagnetic layer of thickness L excited by a controlled time-dependent spin current j_s at the interface $x = 0$ which gives rise to a spin accumulation $m_0(x, t)$, which then diffuses along the x axis, yielding the time-dependent profiles of spin accumulation $m(x, t)$ and induced nonequilibrium chemical potential $\varphi(x, t)$.

where J_{sd} and τ_{sf} represent the s - d exchange constant and spin relaxation time, respectively, and γ is an angle between local magnetization and the x axis. The first equation in (5) expresses the conservation of the charge current, while the second one represents the spin current sinking due to spin-flip processes and precession around the local magnetization. In the collinear case ($\gamma = 0$) the system of Eqs. (5), assuming definitions (4), can be rewritten as

$$\begin{aligned} \frac{\partial n_0}{\partial t} - \frac{\sigma_0}{e} \frac{\partial^2}{\partial x^2} \left(u + \frac{n_0}{eN_0} \right) - \frac{\sigma_0 \beta}{e^2 N_0} \frac{\partial^2 \Delta n}{\partial x^2} &= 0, \\ \frac{\partial \Delta n}{\partial t} - \frac{\sigma_0}{e^2 N_0} \frac{\partial^2 \Delta n}{\partial x^2} - \frac{\sigma_0 \beta}{e} \frac{\partial^2}{\partial x^2} \left(u + \frac{n_0}{eN_0} \right) &= -\frac{\Delta n}{\tau_{sf}}. \end{aligned} \quad (6)$$

To illustrate the dynamic behavior of the spin accumulation, we consider a toy model consisting of a single ferromagnetic layer (FM layer) of thickness L in which a rising time-dependent pure spin current j_s , related to a spin accumulation and proportional to $\partial \Delta n / \partial x$, is injected at the interface $x = 0$ (see Fig. 1). The considered FM layer is similar to the analyzer in the previously studied T-shaped lateral structure [58] in which the chemical potential φ is induced by the pure spin current. Since no bias voltage is applied, the electrostatic potential u is uniform (zero) all along the FM layer. So substituting the conductance \mathcal{D}_0 by a diffusion coefficient \mathcal{D}_0 using Einstein's relation $\mathcal{D}_0 = \sigma_0 / (e^2 N_0)$ and introducing the new functions $\varphi(x, t) = n_0(x, t) / (eN_0)$, the nonequilibrium potential, and $m(x, t) = \Delta n(x, t) / (v/N_0)$, the dimensionless nonequilibrium spin accumulation, where v is the density of states per atom at the Fermi level, we can rewrite (6) in a new form:

$$\begin{aligned} \frac{\partial \varphi(x, t)}{\partial t} - \mathcal{D}_0 \frac{\partial^2 \varphi(x, t)}{\partial x^2} - \frac{\beta \mathcal{D}_0}{ev} \frac{\partial^2 m(x, t)}{\partial x^2} &= 0, \\ \frac{\partial m(x, t)}{\partial t} - \mathcal{D}_0 \frac{\partial^2 m(x, t)}{\partial x^2} - \beta \mathcal{D}_0 ev \frac{\partial^2 \varphi(x, t)}{\partial x^2} &= -\frac{m(x, t)}{\tau_{sf}}. \end{aligned} \quad (7)$$

On the opposite side (i.e., at $x = L$), we assume that the spin accumulation and chemical potential φ are kept equal to zero.

The quasistatic time-dependent functions of the spin accumulation and chemical potential can be expressed using a

characteristic rise time $1/\omega$:

$$\begin{aligned} m_0(x, t) &= \tilde{m}_0(x)(1 - e^{-\omega t}), \\ \varphi_0(x, t) &= \tilde{\varphi}_0(x)(1 - e^{-\omega t}), \end{aligned} \quad (8)$$

where $\tilde{m}_0(x)$ and $\tilde{\varphi}_0(x)$ are the stationary solutions of (7) with boundary conditions $\tilde{m}_0(0) = m_{\max}$, where m_{\max} is defined by the maximum of injected current $j_s \propto \partial \tilde{m}_0 / \partial x$ reached at $t \rightarrow \infty$, and $\tilde{m}_0(L) = 0$:

$$\begin{aligned} \tilde{m}_0(x) &= m_{\max} \frac{\sinh(L-x)/\ell_{sf}}{\sinh L/\ell_{sf}}, \\ \tilde{\varphi}_0(x) &= -\frac{\beta}{ev} \tilde{m}_0(x). \end{aligned} \quad (9)$$

Under this condition, the final solution of Eqs. (7) may be written as

$$\begin{aligned} m_0(x, t) &= m_0(x, t) + \Delta m(x, t), \\ \varphi_0(x, t) &= \varphi_0(x, t) + \Delta \varphi(x, t), \end{aligned} \quad (10)$$

where the functions $\Delta m(x, t)$ and $\Delta \varphi(x, t)$ are solutions of (7) both equal to zero at $x = L$ to satisfy the boundary conditions and their spatial derivatives at $x = 0$ are also equal to zero so that they have no contribution to the injected current j_s :

$$\begin{aligned} \Delta m(x, t) &= \sum_n \int_0^t [b_{1n}(\tau) e^{-E_{1n}(t-\tau)} \\ &\quad + b_{2n}(\tau) e^{-E_{2n}(t-\tau)}] \sin k_n(L-x) d\tau, \\ \Delta \varphi(x, t) &= \sum_n \int_0^t [a_{1n} b_{1n}(\tau) e^{-E_{1n}(t-\tau)} \\ &\quad + a_{2n} b_{2n}(\tau) e^{-E_{2n}(t-\tau)}] \sin k_n(L-x) d\tau, \end{aligned} \quad (11)$$

where

$$\begin{aligned} b_{1n}(\tau) + b_{2n}(\tau) &= -\frac{\partial}{\partial \tau} (1 - e^{-\omega \tau}) m_{0n}, \\ a_{1n} b_{1n}(\tau) + a_{2n} b_{2n}(\tau) &= -\frac{\partial}{\partial \tau} (1 - e^{-\omega \tau}) \varphi_{0n}, \\ m_{0n} &= \frac{1}{L} \int_0^L \tilde{m}_0(x) \sin k_n(L-x) dx, \\ \varphi_{0n} &= \frac{1}{L} \int_0^L \tilde{\varphi}_0(x) \sin k_n(L-x) dx, \\ a_{1,2n} &= \frac{\beta \mathcal{D} k_n^2}{E_{1,2n} - \mathcal{D} k_n^2 ev}, \\ E_{1,2n} &= \mathcal{D} k_n^2 + \frac{1}{2\tau_{sf}} \mp \sqrt{\left(\frac{1}{2\tau_{sf}} \right)^2 + \beta^2 \mathcal{D}^2 k_n^4}, \\ k_n &= \frac{\pi}{2L} (2n+1). \end{aligned} \quad (12)$$

In these expressions, E_{1n} and E_{2n} are sets of inverse characteristic time rates associated with the spin accumulation diffusion process along the ferromagnetic layer thickness for spin up (E_1) and down (E_2). As expected from a diffusion process, the corresponding diffusion times roughly scale as a square of the layer thickness. Finally, after integration (11)

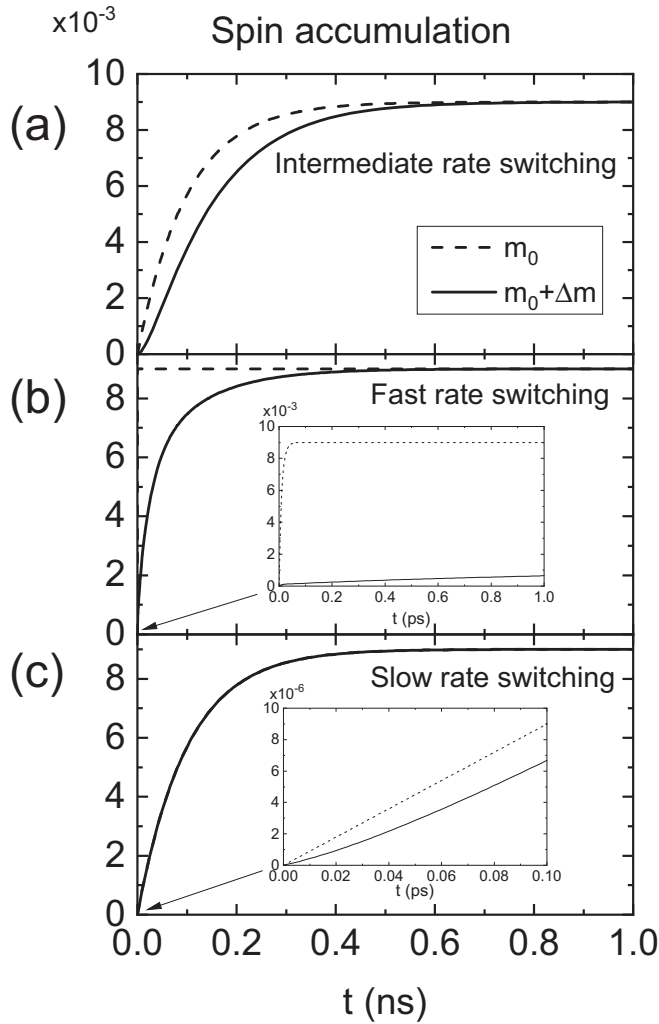


FIG. 2. Dependence of quasistatic m_0 and total dynamic $m_0 + \Delta m$ spin accumulation on time at $x = 0$. Parameters are (a) $L = 500$ nm, $m_0 = 0.009$, $\beta = 0.7$, $\tau_{sf} = 10^{-10}$ s, $\nu = 0.1$ eV $^{-1}$, $\sigma = 0.001$ (ω nm) $^{-1}$, $\omega = 10^{10}$ s $^{-1}$. Characteristic times are $E_1^{-1} \approx 1.14 \times 10^{-10}$ s, $E_2^{-1} \approx 3 \times 10^{-11}$ s, (b) $\omega = 10^{14}$ s $^{-1}$ and (c) $\tau_{sf} = 10^{-14}$ s, $\omega = 10^{10}$ s $^{-1}$, $L = 50$ nm, $E_1^{-1} \approx 6.5 \times 10^{-13}$ s, $E_2^{-1} \approx 5.4 \times 10^{-14}$ s.

over τ , we have

$$\Delta m(x, t) = \sum_n \frac{\sin k_n(L-x)}{a_{1n} - a_{2n}} \omega \times \left[(-\varphi_{0n} + a_{2n}m_{0n}) \frac{e^{-\omega t} - e^{-E_{1n}t}}{E_{1n} - \omega} + (\varphi_{0n} - a_{1n}m_{0n}) \frac{e^{-\omega t} - e^{-E_{2n}t}}{E_{2n} - \omega} \right]. \quad (13)$$

III. RESULTS AND DISCUSSION

In Figs. 2(a)–2(c), the dependencies of the quasistatic and total dynamic spin accumulation at $x = 0$ are plotted versus time for different values of ω and $E_{1,2}$. The black curve represents the time-dependent spin accumulation $m_0(x, t)$ without taking into account the process of diffusion, while the dashed line represents the total spin accumulation $m_0 + \Delta m$. In

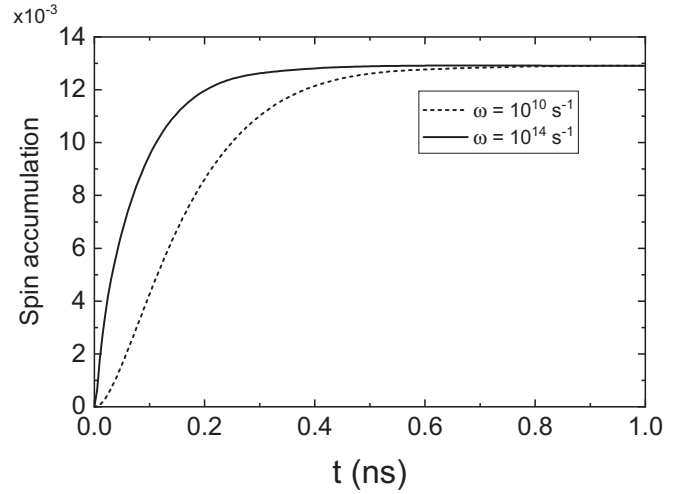


FIG. 3. Numerical dependence of total dynamic spin accumulation $m(x, t)$ on time in spin valve F1/P1/F2/P2 at the F2/P2 interface for two different rise rates ω of the injected spin current.

Fig. 2(a), the characteristic time of the switching ($1/\omega$) is of the same order of magnitude as the characteristic first-order ($n = 0$) time of diffusion ($E_{1,2}^{-1}$). In this case, the diffusion process influences the stabilization of spin accumulation but not substantially. In Fig. 2(b), the same curves are presented but for very fast switching rate $\omega = 10^{14}$ s $^{-1} \gg E_1$ and $E_2 \approx 10^{10}$ s $^{-1}$. In this case, the slow diffusion process dominates, and stabilization of the total process occurs at very long times, longer than $E_1^{-1} \approx 10^{-10}$ s. Finally, the same type of curves as in Figs. 2(a) and 2(b) are presented in Fig. 2(c), in a case where the length (thickness) of the ferromagnetic layer has been reduced to 50 nm instead of 500 nm so that the characteristic diffusion times are reduced to $E_1^{-1} \approx 6.5 \times 10^{-13}$ s, $E_2^{-1} \approx 5.4 \times 10^{-14}$ s. The same rise rate as that used in Fig. 2(a) now corresponds to a slow switching compared to the diffusion time ($\omega^{-1} = 10^{-10}$ s $\gg E_1^{-1}$, $E_2^{-1} \approx 10^{-13}$ s). In this case, the process of diffusion influences the time dependence of spin accumulation only at the very beginning of the diffusion process ($t \sim 10^{-14} - 10^{-13}$ s).

Going beyond the toy model which allowed us to derive analytical expressions, we now numerically investigate the evolution in time of spin accumulation in spin valves of the form F1/P2/F2/P2 using the finite-element method for $\omega = 10^{10}$ and 10^{14} s $^{-1}$ (see Fig. 3). We used a periodic condition for the spin accumulation m at the left F1 and P2 boundary. The chemical potential φ was set equal to zero at the left F1 boundary, and electrical current $\sim \partial\varphi/\partial x$ remained constant at the right P2 boundary. Both curves are similar to the corresponding curves in Figs. 2(a) and 2(b), supporting our conclusion that if time of switching ($1/\omega$) is longer than the characteristic diffusion times, the spin accumulation follows the external signal in a quasistatic manner. However, if this time is shorter than these characteristic times, the evolution of spin accumulation is governed by slow diffusion and spin-relaxation processes.

In Fig. 4, we plot the time $t_{1/2}$ at which spin accumulation at point $x = 0$ reaches half of its maximal value versus the length L of the paramagnetic layer P for high $\omega = 10^{14}$ s $^{-1}$ and for two values of τ_{sf} in the paramagnetic layer.

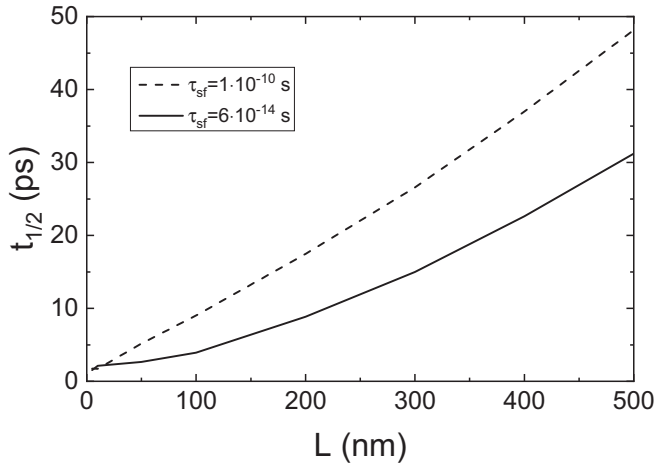


FIG. 4. Time $t_{1/2}$ at which spin accumulation reaches half of its maximum value versus length L of paramagnetic layers P1 and P2 in spin valve F1/P1/F2/P2 at the F2/P2 interface of two values of τ_{sf} . The length of the F layers is 500 nm.

The values of this time are in the interval 10^{-12} – 10^{-10} s, which are much longer than the assumed switching time $\omega^{-1} \sim 10^{-14}$ s. In addition, they depend on both the length of the paramagnetic layer and spin-relaxation time in qualitative agreement with expressions for E_1 and E_2 . This emphasizes that at high excitation frequencies such as in the THz regime or in large-size devices, the spin-accumulation dynamics can be governed by the relatively slow processes of spin relaxation and spin diffusion.

Last, we investigate the dynamics of the spin accumulation in spin valves F1/P1/F2/P2 assuming that the magnetization of F2 rotates with frequency ω while the magnetization of F1 remains fixed. This is in contrast to the method from Ref. [40], where periodically varying voltage was applied. As shown in Fig. 5, the spin accumulation oscillates with

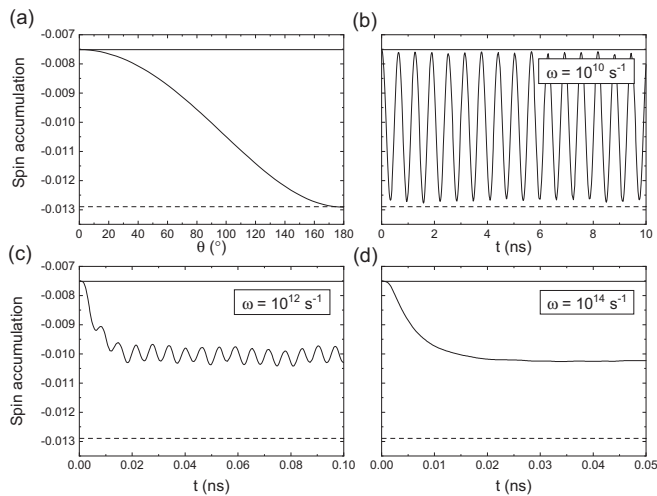


FIG. 5. Spin accumulation at the F1/P1 interface versus (a) the angle θ between magnetizations of ferromagnetic layers F1 and F2 and (b)–(d) time at different rotating frequencies ω of magnetization of ferromagnetic layer F1 in spin valve F1/P1/F2/P2. The length of the F layers is 50 nm, that of the P layers is 500 nm, and $\tau_{sf} = 10^{-10}$ s.

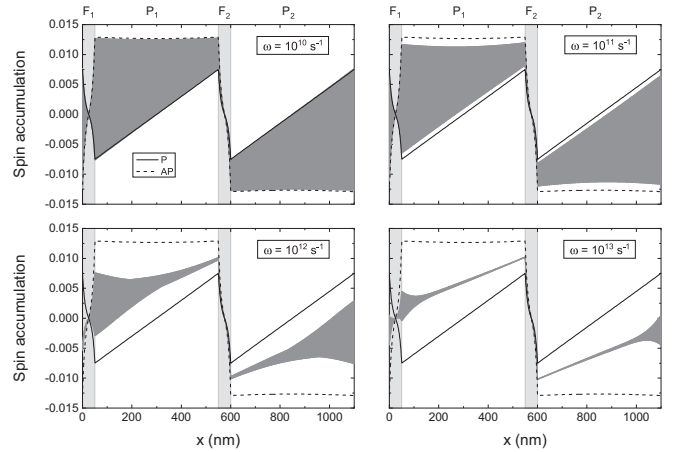


FIG. 6. Distribution of spin accumulation along the spin valve F1/P1/F2/P2 for different rotating frequencies ω of magnetization in ferromagnetic layer F1.

period $2\pi/\omega$. However, as the frequency ω increases [see Figs. 5(b)–5(d)], the amplitude of the oscillations drops due to the slow processes of spin relaxation and spin diffusion ($\tau_{sd} \sim L^2/D \approx 10^{-11}$ s, $\tau_{sf} = 10^{-10}$ s). At high frequency, the spin accumulation reaches an average value corresponding to the average between spin accumulation in parallel and antiparallel alignment.

In Fig. 6, the gray areas correspond to the superposition of all profiles of spin accumulation as the magnetization of F2 rotates for four values of frequency. The dashed and solid lines represent the limiting static profiles in the parallel (solid curve) and antiparallel (dashed curve) configurations. The decrease with frequency of the amplitude of the oscillations of spin accumulation as the magnetization of F2 rotates is clearly visible.

The corresponding curves for the spatial distribution of the electrostatic potential for three frequencies and GMR decay

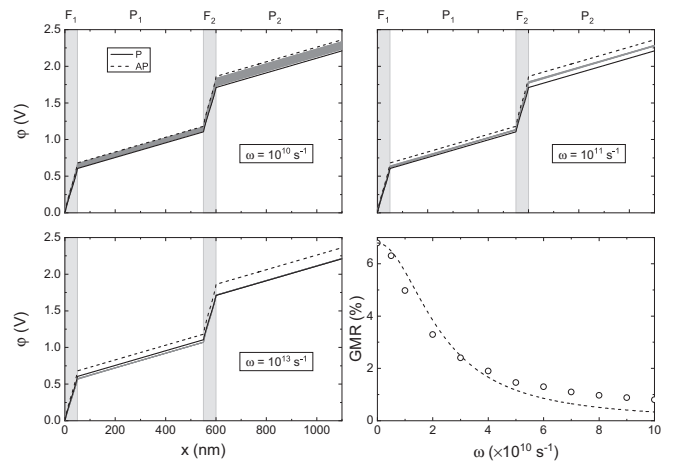


FIG. 7. Distribution of the potential along spin valve F1/P1/F2/P2 for different rotating frequencies ω of magnetization in ferromagnetic layer F1. GMR decay fit by a Lorentzian $GMR(\omega) = GMR_0/(1 + \tau^2\omega^2)$ (dashed line) with $GMR_0 = 6.79\%$, $\tau = 4.4 \times 10^{-11}$ s.

are plotted in Fig. 7. Thin curves show the distribution of the potential for the static case for parallel (solid curve) and antiparallel (dashed curve) orientation of magnetizations of ferromagnetic layers. The width of the inner gray line corresponds to the amplitude of the oscillations of the potential, e.g., the value of the GMR in the dynamic regime. Under the assumption of the model, the amplitude of the GMR was found to decrease with frequency approximately as a function of the form $\text{GMR}(\omega) \approx \text{GMR}_0/(1 + \tau^2\omega^2)$ ($\tau = 4.4 \times 10^{-11}$ s) similar to the real part of the frequency-dependent conductivity (2). Actually, recent GMR measurements at THz frequency were reported in Ref. [39] in multilayers of composition Ta (5 nm)/NiFeCo (4 nm)/[Cu (1.3 nm)/NiCoFe (2.6 nm)]₃/Cu (1.3 nm)/NiFeCo (4 nm)/Cu (1.2 nm)/NiFeCo (0.8 nm). The GMR measured by the terahertz magnetospectroscopy experiment ($\sim 20\%$) was quite comparable to that measured in DC mode (22%). This is actually in agreement with the present model since the thickness of the Cu spacers over which the electrons have to diffuse to produce the GMR effect is only 1.2 nm, meaning that the diffusion time is quite short compared to the THz excitation frequency. It would be interesting to perform similar experiments in nonlocal geometry with a much longer spin channel to observe the reduction of the nonlocal spin signal due to diffusion time becoming comparable to characteristic excitation times.

IV. CONCLUSION

We have shown that the dynamics of spin accumulation in metallic spintronic devices can be significantly slower than typical elastic scattering times in metals. This is due to the fact that spin accumulation variation results from a spin diffusion process which itself involves numerous individual scattering events. This can have important consequences for spintronic devices operating in the THz regime or more generally in devices in which the excitation characteristic time would be comparable to or shorter than the characteristic spin diffusion time in the device. In spin-valve structures, particularly lateral spin-valve structures of large dimension (e.g., hundreds of nanometers), the time evolution of the output signal is controlled by the slowest process (e.g., diffusion), so it leads to the limitations in read and write speed in spintronic devices, and the measured amplitude of the magnetosensitive output signal can consequently depend on the frequency of the excitations.

ACKNOWLEDGMENTS

This work was funded under ERC Adv Grant No. MAGICAL 669204. A.V. and A.L. are grateful to the Russian Foundation for Basic Research for the support through Grant No. 19-02-00316-A.

- [1] E. Beaupaire, J.-C. Merle, A. Daunois, and J.-Y. Bigot, *Phys. Rev. Lett.* **76**, 4250 (1996).
- [2] C. D. Stanciu, F. Hansteen, A. V. Kimel, A. Kirilyuk, A. Tsukamoto, A. Itoh, and T. Rasing, *Phys. Rev. Lett.* **99**, 047601 (2007).
- [3] J. Walowski and M. Münzenberg, *J. Appl. Phys.* **120**, 140901 (2016).
- [4] A. Kirilyuk, A. V. Kimel, and T. Rasing, *Rev. Mod. Phys.* **82**, 2731 (2010).
- [5] J.-Y. Bigot and M. Vomir, *Ann. Phys. (Berlin, Ger.)* **525**, 2 (2013).
- [6] M. Tonouchi, *Nat. Photonics* **1**, 97 (2007).
- [7] J. C. Slonczewski, *J. Magn. Magn. Mater.* **159**, L1 (1996).
- [8] L. Berger, *Phys. Rev. B* **54**, 9353 (1996).
- [9] M. Kreissig, R. Lebrun, F. Protze, K. J. Merazzo, J. Hem, L. Vila, R. Ferreira, M. C. Cyrille, F. Ellinger, V. Cros, U. Ebels, and P. Bortolotti, *AIP Adv.* **7**, 056653 (2017).
- [10] L. Liu, C.-F. Pai, D. C. Ralph, and R. A. Buhrman, *Phys. Rev. Lett.* **109**, 186602 (2012).
- [11] V. E. Demidov, S. Urazhdin, H. Ulrichs, V. Tiberkevich, A. Slavin, D. Baither, G. Schmitz, and S. O. Demokritov, *Nat. Mater.* **11**, 1028 (2012).
- [12] M. Zahedinejad, A. A. Awad, S. Muralidhar, R. Khymyn, H. Fulara, H. Mazraati, M. Dvornik, and J. Åkerman, *Nat. Nanotech.* (2019), doi: [10.1038/s41565-019-0593-9](https://doi.org/10.1038/s41565-019-0593-9).
- [13] A. Ruiz-Calaforra, A. Purbawati, T. Brächer, J. Hem, C. Murapaka, E. Jiménez, D. Mauri, A. Zeltser, J. A. Katine, M.-C. Cyrille, L. D. Buda-Prejbeanu, and U. Ebels, *Appl. Phys. Lett.* **111**, 082401 (2017).
- [14] R. Lebrun, S. Tsunegi, P. Bortolotti, H. Kubota, A. S. Jenkins, M. Romera, K. Yakushiji, A. Fukushima, J. Grollier, S. Yuasa, and V. Cros, *Nat. Commun.* **8**, 15825 (2017).
- [15] H. S. Choi, S. Y. Kang, S. J. Cho, I.-Y. Oh, M. Shin, H. Park, C. Jang, B.-C. Min, S.-I. Kim, S.-Y. Park, and C. S. Park, *Sci. Rep.* **4**, 5486 (2015).
- [16] S. Tsunegi, T. Taniguchi, R. Lebrun, K. Yakushiji, V. Cros, J. Grollier, A. Fukushima, S. Yuasa, and H. Kubota, *Sci. Rep.* **8**, 13475 (2018).
- [17] A. A. Tulapurkar, Y. Suzuki, A. Fukushima, H. Kubota, H. Maehara, K. Tsunekawa, D. D. Djayaprawira, N. Watanabe, and S. Yuasa, *Nature (London)* **438**, 339 (2005).
- [18] S. Miwa, S. Ishibashi, H. Tomita, T. Nozaki, E. Tamura, K. Ando, N. Mizuochi, T. Saruya, H. Kubota, K. Yakushiji, T. Taniguchi, H. Imamura, A. Fukushima, S. Yuasa, and Y. Suzuki, *Nat. Mater.* **13**, 50 (2014).
- [19] B. Fang, M. Carpentieri, X. Hao, H. Jiang, J. A. Katine, I. N. Krivorotov, B. Ocker, J. Langer, K. L. Wang, B. Zhang, B. Azzerboni, P. K. Amiri, G. Finocchio, and Z. Zeng, *Nat. Commun.* **7**, 11259 (2016).
- [20] G. A. Akpakwu, B. J. Silva, G. P. Hancke, and A. M. Abu-Mahfouz, *IEEE Access* **6**, 3619 (2018).
- [21] S. Mizukami, A. Sugihara, S. Iihama, Y. Sasaki, K. Z. Suzuki, and T. Miyazaki, *Appl. Phys. Lett.* **108**, 012404 (2016).
- [22] O. R. Sulymenko, O. V. Prokopenko, V. S. Tyberkevych, and A. N. Slavin, *IEEE Magn. Lett.* **9**, 3104605 (2018).
- [23] M. Battiato, K. Carva, and P. M. Oppeneer, *Phys. Rev. Lett.* **105**, 027203 (2010).
- [24] M. Battiato, K. Carva, and P. M. Oppeneer, *Phys. Rev. B* **86**, 024404 (2012).
- [25] T. Kampfrath, M. Battiato, P. Maldonado, G. Eilers, J. Nötzold, S. Mährlein, V. Zbarsky, F. Freimuth, Y. Mokrousov, S. Blügel, M. Wolf, I. Radu, P. M. Oppeneer, and M. Münzenberg, *Nat. Nanotechnol.* **8**, 256 (2013).
- [26] N. F. Mott, *Proc. R. Soc. London, Ser. A* **153**, 699 (1936).

- [27] P. Drude, *Ann. Phys. (Berlin, Ger.)* **306**, 566 (1900).
- [28] A. Fert and I. A. Campbell, *Phys. Rev. Lett.* **21**, 1190 (1968).
- [29] A. Fert and I. A. Campbell, *J. Phys. Colloq.* **32**, C1-46 (1971).
- [30] A. Fert and I. A. Campbell, *J. Phys. F* **6**, 849 (1976).
- [31] I. A. Campbell and A. Fert, *Transport Properties of Ferromagnets* (North Holland, Amsterdam, 1982).
- [32] N. Laman and D. Grischkowsky, *Appl. Phys. Lett.* **93**, 051105 (2008).
- [33] E. E. Fullerton and J. R. Childress, *Proc. IEEE* **104**, 1787 (2016).
- [34] M. Scheffler, M. Dressel, M. Jourdan, and H. Adrian, *Nature (London)* **438**, 1135 (2005).
- [35] N. W. Ashcroft and N. D. Mermin, *Solid State Physics* (Saunders College, Fort Worth, 1976).
- [36] J. M. Ziman, *Principles of the Theory of Solids*, 2nd ed. (Cambridge University Press, Cambridge, 1972).
- [37] M. Dressel and G. Gruner, *Electrodynamics of Solids* (Cambridge University Press, Cambridge, 2002).
- [38] T. Kampfrath, K. Tanaka, and K. A. Nelson, *Nat. Photonics* **7**, 680 (2013); **7**, 665 (2013).
- [39] Z. Jin, A. Tkach, F. Casper, V. Spetter, H. Grimm, A. Thomas, T. Kampfrath, M. Bonn, M. Kläui, and D. Turchinovich, *Nat. Phys.* **11**, 761 (2015).
- [40] D. Kochan, M. Gmitra, and J. Fabian, *Phys. Rev. Lett.* **107**, 176604 (2011).
- [41] W. P. Pratt, S.-F. Lee, J. M. Slaughter, R. Loloee, P. A. Schroeder, and J. Bass, *Phys. Rev. Lett.* **66**, 3060 (1991).
- [42] J. Bass and W. Pratt, *J. Magn. Magn. Mater.* **200**, 274 (1999).
- [43] A. Fert and L. Piraux, *J. Magn. Magn. Mater.* **200**, 338 (1999).
- [44] J. Bass, *J. Magn. Magn. Mater.* **408**, 244 (2016).
- [45] T. Valet and A. Fert, *Phys. Rev. B* **48**, 7099 (1993).
- [46] T. Kimura and Y. Otani, *Phys. Rev. Lett.* **99**, 196604 (2007).
- [47] T. Kimura and Y. Otani, *J. Phys.: Condens. Matter* **19**, 165216 (2007).
- [48] T. Kimura, T. Sato, and Y. Otani, *Phys. Rev. Lett.* **100**, 066602 (2008).
- [49] E. Villamor, M. Isasa, L. E. Hueso, and F. Casanova, *Phys. Rev. B* **87**, 094417 (2013).
- [50] H. Idzuchi, Y. Fukuma, and Y. Otani, *Sci. Rep.* **2**, 628 (2012).
- [51] E. Villamor, M. Isasa, L. E. Hueso, and F. Casanova, *Phys. Rev. B* **88**, 184411 (2013).
- [52] P. Laczkowski, L. Vila, V.-D. Nguyen, A. Marty, J.-P. Attane, H. Jaffres, J.-M. George, and A. Fert, *Phys. Rev. B* **85**, 220404(R) (2012).
- [53] W. Savero Torres, P. Laczkowski, V. D. Nguyen, J. C. Rojas Sanchez, L. Vila, A. Marty, M. Jamet, and J. P. Attane, *Nano Lett.* **14**, 4016 (2014).
- [54] V. T. Pham, L. Vila, G. Zahnd, A. Marty, W. Savero-Torres, M. Jamet, and J.-P. Attané, *Nano Lett.* **16**, 6755 (2016).
- [55] G. Zahnd, L. Vila, V. T. Pham, A. Marty, C. Beigné, C. Vergnaud, and J. P. Attané, *Sci. Rep.* **7**, 9553 (2017).
- [56] P. C. van Son, H. van Kempen, and P. Wyder, *Phys. Rev. Lett.* **58**, 2271 (1987).
- [57] N. Strelkov, A. Vedyayev, N. Ryzhanova, D. Gusakova, L. D. Buda-Prejbeanu, M. Chshiev, S. Amara, N. deMestier, C. Baraduc, and B. Dieny, *Phys. Rev. B* **84**, 024416 (2011).
- [58] A. Vedyayev, N. Ryzhanova, N. Strelkov, T. Andrianov, A. Lobachev, and B. Dieny, *Phys. Rev. Appl.* **10**, 064047 (2018).